Investigating Nuclear Shell Structure in the Vicinity of ^{78}Ni: Low-Lying Excited States in the Neutron-Rich Isotopes ^{80,82}Zn

Y. Shiga,[1,2,*] K. Yoneda,[2] D. Steppenbeck,[2] N. Aoi,[3] P. Doornenbal,[2] J. Lee,[2,†] H. Liu,[2,4] M. Matsushita,[2,‡] S. Takeuchi,[2,§] H. Wang,[2,4] H. Baba,[2] P. Bednarczyk,[5] Zs. Dombradi,[6] Zs. Fulop,[6] S. Go,[2,7,¶] T. Hashimoto,[3] M. Honma,[8] E. Ideguchi,[7] K. Ieki,[1] K. Kobayashi,[1] Y. Kondo,[9,2] R. Minakata,[9,2] T. Motobayashi,[2] D. Nishimura,[2,**] T. Otsuka,[7,10] H. Otsu,[2] H. Sakurai,[2,10] N. Shimizu,[7] D. Sohler,[6] Y. Sun,[11] A. Tamii,[3] R. Tanaka,[9,2] Z. Tian,[4] Y. Tsunoda,[12] Zs. Vajta,[6] T. Yamamoto,[3] X. Yang,[2,††] Z. Yang,[2] Y. Ye,[4] R. Yokoyama,[2,7] and J. Zenihiro[2]

[1] *Department of Physics, Rikkyo University, Toshima, Tokyo 171-8501, Japan*
[2] *RIKEN Nishina Center, 2-1, Hirosawa, Wako, Saitama 351-0198, Japan*
[3] *Research Center for Nuclear Physics, Osaka University, Ibaraki, Osaka 567-0047, Japan*
[4] *School of Physics, Peking University, 209 Chengfu Rd, Beijing 100871, People's Republic of China*
[5] *Institute of Nuclear Physics, Polish Academy of Sciences, 152 Radzikowskiego St., Krakow 31-342, Poland*
[6] *Institute for Nuclear Research, P.O. Box 51, Debrecen 4001, Hungary*
[7] *Center for Nuclear Study, University of Tokyo, RIKEN campus, Wako, Saitama 351-0198, Japan*
[8] *Center for Mathematical Sciences, University of Aizu, Ikki-machi, Aizu-Wakamatsu, Fukushima 965-8580, Japan*
[9] *Department of Physics, Tokyo Institute of Technology, Meguro, Tokyo 152-8551, Japan*
[10] *Department of Physics, University of Tokyo, Hongo, Bunkyo, Tokyo 113-0033, Japan*
[11] *Department of Physics, Shanghai Jiao-Tong University, Shanghai 200240, People's Republic of China*
[12] *Center for Nuclear Study, University of Tokyo, Hongo, Bunkyo-ku, Tokyo 113-0033, Japan*

(Dated: November 11, 2015)

The low-lying level structures of nuclei in the vicinity of ^{78}Ni were investigated using in-beam γ-ray spectroscopy to clarify the nature of the nuclear magic numbers $Z = 28$ and $N = 50$ in systems close to the neutron dripline. Nucleon knockout reactions were employed to populate excited states in ^{80}Zn and ^{82}Zn. A candidate for the 4_1^+ level in ^{80}Zn was identified at 1979(30) keV, and the lifetime of this state was estimated to be 136^{+92}_{-67} ps from a line-shape analysis. Moreover, the energy of the 2_1^+ state in ^{82}Zn is reported to lie at 621(11) keV. The large drop in the 2_1^+ energy at ^{82}Zn indicates the presence of a significant peak in the $E(2_1^+)$ systematics at $N = 50$. Furthermore, the $E(4_1^+)/E(2_1^+)$ and $B(E2; 4_1^+ \rightarrow 2_1^+)/B(E2; 2_1^+ \rightarrow 0^+_{\mathrm{g.s.}})$ ratios in ^{80}Zn were deduced to be 1.32(3) and 1.12^{+80}_{-60}, respectively. These results imply that ^{80}Zn can be described in terms of two-proton configurations with a ^{78}Ni core, and are consistent with a robust $N = 50$ magic number along the Zn isotopic chain. These observations, therefore, indicate a persistent $N = 50$ shell closure in nuclei far from the line of β stability, which in turn suggests a doubly magic structure for ^{78}Ni.

PACS numbers: 23.20.Lv, 27.50.+e, 29.38.Db

The evolution of nuclear shell structure in exotic, neutron-rich atomic nuclei has been at the forefront of nuclear physics research for several decades. The shell model, which was originally proposed by Mayer and Jensen [1, 2], succeeded in reproducing the conventional nuclear magic numbers (N, Z = 2, 8, 20, 28, 50, and 82), as well as other nuclear properties in the vicinity of the valley of stability. However, it was later discovered that conventional shell structure is not necessarily valid in regions far from the valley of stability. Indeed, recent developments in accelerator technology and isotope separators have made it possible to explore uncharted regions of the Segrè chart, yielding many new, exotic phenomena that cannot be explained in the framework of the standard shell model. Several highlights include the weakening of the traditional magic numbers $N = 8$ [3–5], 20 [6], and 28 [7–9], while new magic numbers at $N = 16$ [10, 11], 32 [12–20], and 34 [21] have been reported. The next conventional neutron magic number, $N = 50$, has also attracted much attention recently, and investigations into the robustness of this magic number in neutron-rich systems has been encouraged.

The persistence of the $N = 50$ magic number in exotic regions also bears particular importance in the field of nuclear astrophysics. The rapid neutron-capture (r) process [22], which is believed to be a major process in the synthesis of the elements heavier than Fe, passes through the neutron-rich regions, and the so-called waiting points exist at the nuclear magic numbers. Thus, the strength of the $N = 50$ shell closure in exotic nuclei is important for gaining a more complete understanding of nucleosynthesis and the resulting natural abundances of the elements [23].

The ^{78}Ni nucleus, having the conventional proton and neutron magic numbers $Z = 28$ and $N = 50$, is located in a region very far from the line of β stability. Much ef-

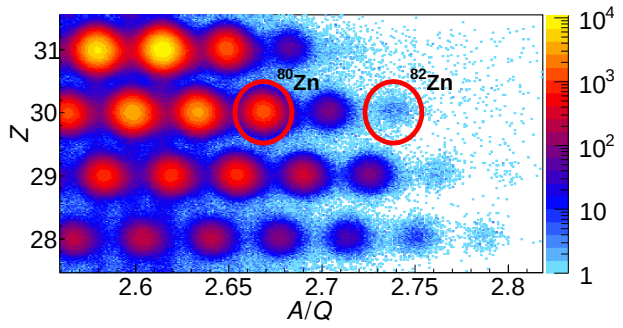

FIG. 1. (color online). Particle identification plot, displaying the mass-to-charge ratio (A/Q) versus atomic number (Z), for radioactive ions identified using the ZeroDegree spectrometer. The red circles indicate ^{80}Zn and ^{82}Zn.

fort has been afforded on both the experimental [24, 25] and theoretical [26, 27] fronts to clarify the mechanism of shell evolution in and around ^{78}Ni; however, direct evidence regarding the magicity of this nucleus is yet to be reported. Moreover, an inversion of the effective single-particle energies between the $\pi p_{3/2}$ and $\pi f_{5/2}$ proton orbitals has been predicted [28] in this neutron-rich region. This inversion has already been confirmed in ^{75}Cu via measurements of the magnetic moment and spin using a combination of collinear and in-source laser spectroscopy [29].

In addition, some of the major consequences of shell evolution can present themselves in the systematics of low-lying nuclear excited states. The energy of the first 2^+ state [$E(2_1^+)$], and the $E(4_1^+)/E(2_1^+)$ energy ratio ($R_{4/2}$), are sensitive to nuclear collectivity and magicity. In earlier studies, $E(2_1^+)$ and reduced transition probabilities, $B(E2; 2_1^+ \rightarrow 0_{\rm g.s.}^+)$ [$\equiv B(E2\downarrow)$], were measured along the $Z = 30$ isotopic chain up to ^{80}Zn ($N = 50$) [30, 31]. The energy of the 2_1^+ state in ^{80}Zn was found to be higher than those of the neighboring even-even Zn isotopes; Ref. [30] also reported that the $B(E2\downarrow)$ systematics can be interpreted successfully assuming a strong $Z = 28$ core polarization through a comparison with shell-model calculations. Additional experimental information that will shed light on the structures of nuclei around ^{78}Ni is awaited.

The present Letter reports on excited states in ^{80}Zn, which is one of the closest even-even neighbors to ^{78}Ni on the Segrè chart, and a new transition in ^{82}Zn is presented. The systematic trends of $E(2_1^+)$, $E(4_1^+)$, and $R_{4/2}$ are discussed and compared to large-scale shell-model calculations [26, 32]. As a result, the evolution of shell structure in the vicinity of doubly magic ^{78}Ni is examined.

The experiment was performed at the Radioactive Isotope Beam Factory, operated by the RIKEN Nishina Center and the Center for Nuclear Study, University of Tokyo. The nuclei of interest—neutron-rich systems near ^{78}Ni—were produced via projectile fragmentation of a 345 MeV/nucleon ^{238}U primary beam with a typical intensity of ~ 2 pnA. The fragment products, which were produced in a 925-mg/cm^2 ^{9}Be target, were separated and identified on an event-by-event basis using projectile times of flight (ToF), magnetic rigidities ($B\rho$), and energy losses in a segmented ionization chamber (ΔE) in the BigRIPS separator [33]; the large acceptance of the spectrometer allowed for the transportation of a variety of nuclei around ^{78}Ni. The main constituents of the secondary radioactive isotope (RI) beam were ^{82}Ge and ^{83}As, both with purities of $\sim 20\%$. The RI beam was delivered to a secondary ^{9}Be target with a thickness of 1.89 g/cm^2, located at the eighth focal plane of BigRIPS. The typical mid-target energy of the RI projectiles were about 250 MeV/nucleon. The reaction products were identified using the ZeroDegree spectrometer [33]; the particle identification plot, which was also constructed using the event-by-event, ToF–$B\rho$–ΔE method, is provided in Fig. 1. It is noted that the separation in A/Q between neighboring isotopes is 6σ. In the present work, the BigRIPS and ZeroDegree spectrometers were optimized for transmission of ^{79}Cu and ^{78}Ni, respectively.

The γ-ray detector array DALI2 [34], which surrounded the secondary ^{9}Be reaction target, was employed to measure γ rays emitted from nuclear excited states populated by the reactions. DALI2 consisted of 186 NaI(Tl) detectors covering angles of $\sim 18°$–$148°$ relative to the beam line. The secondary target was mounted inside a 5-mm-thick Al beam pipe, which was covered on the outside by 1-mm-thick Sn and Pb sheets to reduce atomic background. The energy resolution and full-energy-peak efficiency for a 1-MeV γ ray were 8.4% (FWHM) and 17.8%, respectively. The efficiency of the array was estimated using Monte Carlo simulations with the GEANT4 toolkit [35]; simulated spectra were compared to those obtained with standard (stationary) calibration sources (^{60}Co, ^{88}Y, and ^{137}Cs), and the efficiencies were found to agree within 10%. This value was adopted as part of the systematic uncertainty in the γ-ray relative intensity measurements.

Figure 2 displays Doppler-shift corrected γ-ray energy spectra deduced from the ^{9}Be(^{80}Zn,^{80}Zn+γ) and ^{9}Be(^{81}Ga,^{80}Zn+γ) reactions. A coincidence timing window between particle and γ-ray detection of 10 ns was adopted. The energy spectra were fitted with γ-ray response functions generated from GEANT4 simulations, in addition to exponential functions for the background component. The energy of the $2_1^+ \rightarrow 0_{\rm g.s.}^+$ transition in ^{80}Zn is 1497(22) keV from the energy spectrum deduced from the inelastic scattering reaction, ^{9}Be(^{80}Zn, ^{80}Zn+γ)X [see Fig. 2(a)]. The value is consistent with the result of a previous study, which reported the $2_1^+ \rightarrow 0_{\rm g.s.}^+$ transition at 1492(1) keV [30]. The uncertainty of the 1497-keV transition in the present study includes systematic and statistical errors. The systematic error was

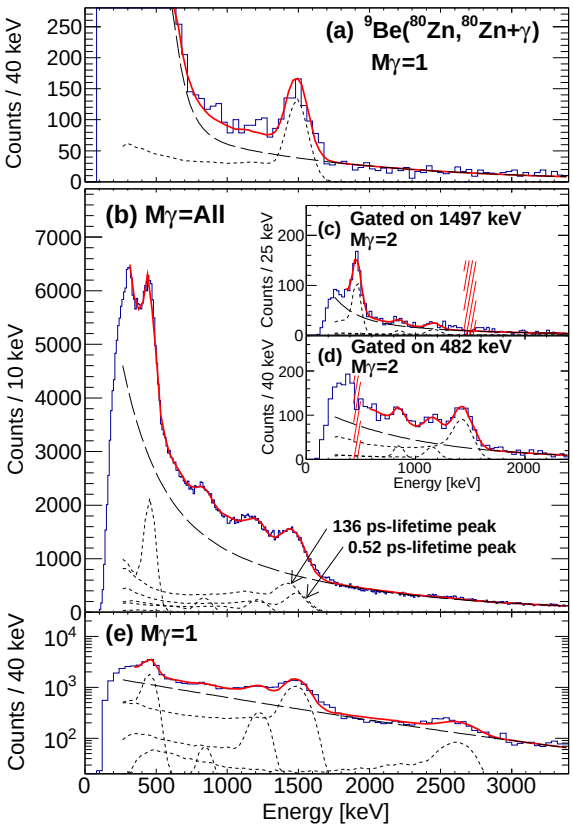

FIG. 2. (color online). Doppler-shift corrected γ-ray energy spectra for ^{80}Zn. (a) Energy spectrum deduced from ^{9}Be(^{80}Zn,^{80}Zn+γ) inelastic scattering reactions for $M_\gamma = 1$ events fitted with a GEANT4 response function (dotted line) and a double exponential function (dashed curve) for a background components. The spectra in panels (b), (c), (d), and (e) were all obtained from ^{9}Be(^{81}Ga,^{80}Zn+γ) proton-removal reactions; (b) and (e) indicate the energy spectra deduced from $M_\gamma \geq 1$ and $M_\gamma = 1$ events, respectively; the insets presented in (c) and (d) indicate the γ rays measured in coincidence with the 1497- and 482-keV peaks, respectively, for $M_\gamma = 2$ events. The hatched areas indicate the widths of the energy gates adopted in the $\gamma\gamma$ coincidence measurements.

estimated by taking the differences between γ-ray transition energies reported in the literature [36] and the results of the present data; this component of the systematic error was deduced to be 1.5%. The peak at $\sim$ 1.5 MeV in Fig. 2(b) corresponds to the $2^+_1 \rightarrow 0^+_{\rm g.s.}$ transition; however, the peak position is shifted down in energy, and its width is larger relative to the inelastic scattering spectrum. In order to disentangle the different components of the spectrum in Fig. 2(b), $\gamma\gamma$ coincidence relationships were investigated. Figure 2(c) indicates the γ rays measured in coincidence with the 1497-keV peak; it is noted that only the events with a γ-ray detection multiplicity of two ($M_\gamma = 2$) were selected. The peak at 482 keV is the strongest amongst all peaks in the coincidence spectrum. As nucleon knockout reactions are known to populate yrast states effectively [9, 37–40], the 482-keV transition is a plausible candidate for the $4^+_1 \rightarrow 2^+_1$ transition. The γ rays measured in coincidence with the 482-keV peak are displayed in the spectrum of Fig. 2(d), which suggests that the 841- and 1195-keV transitions form decay cascades with the 482-keV γ ray. Regarding the energy shift of the 1497-keV peak, a line-shape analysis was performed assuming a relatively long lifetime ($\sim$ 100 ps) for the 482-keV transition, owing to the rather low energy of the $(4^+_1) \rightarrow 2^+_1$ transition. The long lifetime causes appreciable shifts in the points of emission of the γ rays, which in turn affects the angles adopted in the Doppler-shift correction [41]. Considering this effect, the lifetime of the 482-keV state was estimated to be 136^{+92}_{-67} ps using the χ^2 minimization technique with GEANT4 simulated response functions for the $2^+_1 \rightarrow 0^+_{\rm g.s.}$ transition. The uncertainty of the lifetime includes a systematic error induced from the energy determination. The corresponding $B(E2; 4^+_1 \rightarrow 2^+_1)$ value is 162^{+110}_{-81} e^2fm^4. It should be noted that the lifetime of the 2^+_1 state deduced from $B(E2\downarrow) = 144$ e^2fm^4 [31] is 0.52 ps, which is too short to have a significant effect on the line shape. In Fig. 2(e), the ^{9}Be(^{81}Ga,^{80}Zn+γ) spectrum obtained from $M_\gamma = 1$ events is provided, where the $2^+_1 \rightarrow 0^+_{\rm g.s.}$ transition is enhanced, and the peak at 2627(39) keV, which is obscured in Fig. 2(b), becomes clearer. It is stressed here that the spectrum in Fig. 2(b) was fitted using simulated γ-ray response functions assuming unique lifetimes for the 482-, 841-, 1195-, and 2627-keV transitions, while the response function of the 1497-keV γ ray includes the short and long lifetime components discussed above.

In Fig. 3, Doppler-shift corrected γ-ray energy spectra for ^{76,78,82}Zn and ^{82}Ge are presented, which were obtained from the ^{9}Be(X,^{76}Zn+γ), ^{9}Be(^{80}Ga,^{78}Zn+γ), ^{9}Be(X,^{82}Zn+γ), and sum of the ^{9}Be(^{83}Ge,^{82}Ge+γ) and ^{9}Be(^{83}As,^{82}Ge+γ) reactions, respectively. The γ-ray energies deduced from these spectra are summarized in Table I. The most intense peak in each spectrum, after correcting for γ-ray detector efficiencies, is assigned as the $2^+_1 \rightarrow 0^+_{\rm g.s.}$ transition. The observed peaks exhibit a significance larger than 3σ. In Table I, the γ-ray intensities (I_γ) are given relative to the $2^+_1 \rightarrow 0^+_{\rm g.s.}$ transitions for each nucleus. It is noted that $E(2^+_1)$ for ^{76,78}Zn and ^{82}Ge are in good agreement with previous reports [31, 42–45]. In the ^{82}Zn spectrum [Fig. 3(c)], a peak at 621(11) keV, which is assigned as the $2^+_1 \rightarrow 0^+_{\rm g.s.}$ transition, is reported for the first time. The respective γ-ray energy spectra measured in coincidence with the $2^+_1 \rightarrow 0^+_{\rm g.s.}$ transitions in ^{76,78}Zn and ^{82}Ge are presented in the insets of Figs. 3(a), 3(b), and 3(d). The strongest peaks in the coincidence spectra are assigned as $4^+_1 \rightarrow 2^+_1$ transitions, and the spin-parity assignments are consistent with the results of previous studies [31, 42–45].

Figure 4 provides a comparison between the experimental and shell-model level schemes of ^{80}Zn. The

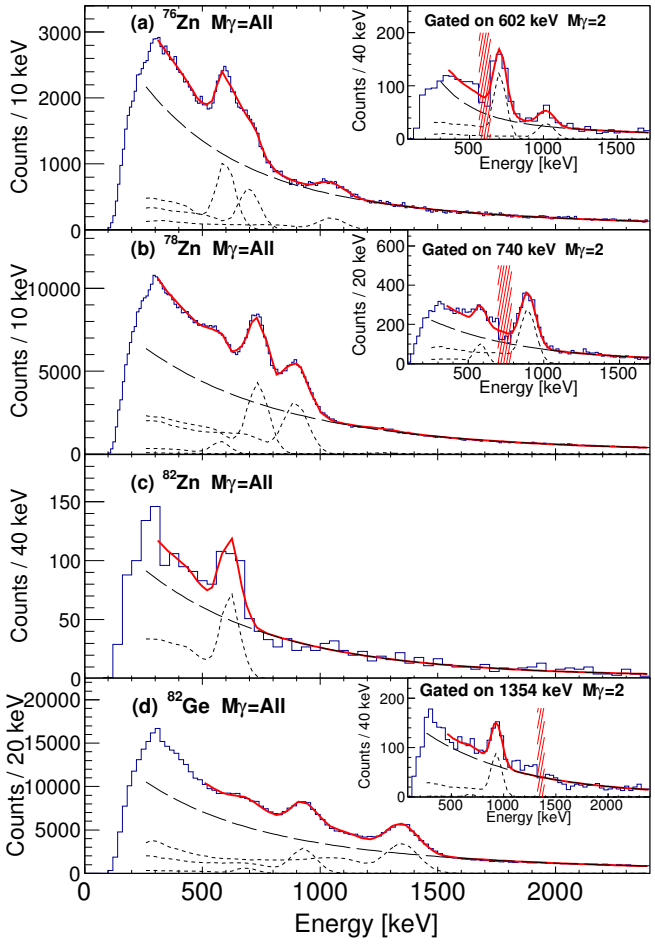

FIG. 3. (color online). (a) Doppler-shift corrected γ-ray energy spectra for $M_\gamma \geq 1$ events observed in the (a) ^{9}Be(X,^{76}Zn+γ), (b) ^{9}Be(^{80}Ga,^{78}Zn+γ), (c) ^{9}Be(X,^{82}Zn+γ), and (d) sum of the ^{9}Be(^{83}Ge,^{82}Ge+γ) and ^{9}Be(^{83}As,^{82}Ge+γ) reaction channels. The insets of panels (a), (b), and (d) are $\gamma\gamma$ coincidence spectra deduced from $M_\gamma = 2$ events with γ gates set on the 602, 740, and 1354 keV transitions, respectively; the hatched areas indicate the widths of the energy gates.

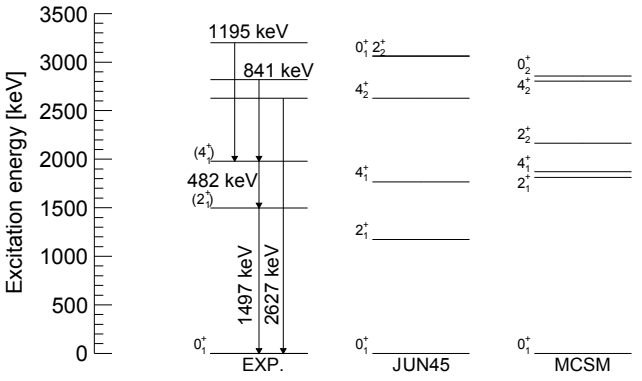

FIG. 4. Level scheme for ^{80}Zn deduced in the present Letter (EXP). Note that the experimental spin-parity assignments are tentative. The shell-model calculations show predictions of the JUN45 interaction [32] and the MCSM [26] (see text for details).

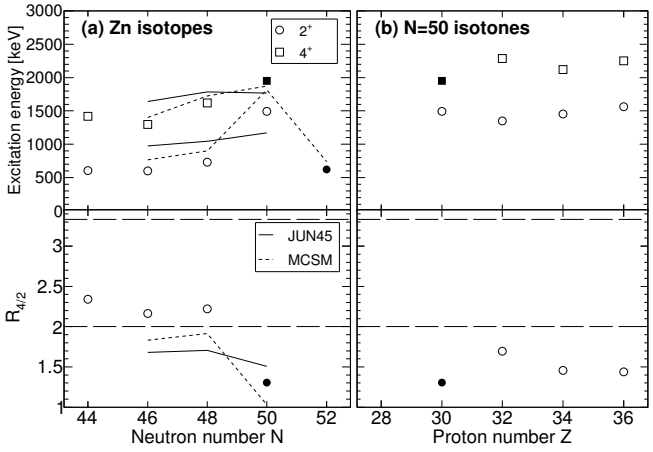

FIG. 5. Systematics of excitation energies for 2_1^+ and 4_1^+ states (top panels), and $R_{4/2}$ (bottom panels) for the (a) Zn isotopic chain and (b) $N = 50$ isotonic chain. The filled symbols indicate results obtained in the present Letter, while other data were taken from Ref. [36]. The solid and short-dashed lines are JUN45 and MCSM calculations, respectively. In the two bottom panels, the horizontal long-dashed lines at 2.00 and 3.33 indicate the vibrational and rotational limits, respectively.

calculations employing the JUN45 interaction adopted a model space consisting of the $1p_{3/2}, 0f_{5/2}, 1p_{1/2}$, and $0g_{9/2}$ orbitals [32]. The MCSM calculations were performed using the advanced Monte Carlo Shell Model with the K computer [26], and employed a model space that contained the full pf shell and the $0g_{9/2}$ and $1d_{5/2}$ orbitals. Both calculations predict that the 4_1^+ level lies closest in energy to the 2_1^+ level, and the predicted energies are in reasonable agreement with the experimental values. Note that the $R_{4/2}$ ratio, which is deduced to be 1.31(2), is rather small, even compared to the ideal vibrational limit of 2.00. The origin of such small $R_{4/2}$ value is likely to be the neutron shell closure at $N = 50$. Moreover, the $B(E2; 4_1^+ \rightarrow 2_1^+)/B(E2; 2_1^+ \rightarrow 0_{\rm g.s.}^+)$ ratio, which is reported to be 1.12^{+80}_{-60} in the present Letter, is consistent with value [46, 47] obtained for two-particle configurations in seniority scheme with $\nu = 2$. Thus, the shell structure of ^{80}Zn can be depicted as two-proton configurations with a ^{78}Ni core.

The systematic trends of $E(2_1^+)$, $E(4_1^+)$, and $R_{4/2}$ along the Zn isotopic and $N = 50$ isotonic chains are displayed in Figs. 5(a) and 5(b), respectively. It is apparent from Fig. 5(a) that the 2_1^+ energy of ^{82}Zn is notably lower than that of ^{80}Zn and comparable to the values in ^{74,76,78}Zn, thus indicating a local maximum at $N = 50$.

TABLE I. Summary of γ-ray transitions in ^{76,78,80,82}Zn and ^{82}Ge observed in the present study. The γ-ray energies from previous studies are included for reference.

	γ-ray energy (keV)			Transition	
Isotope	Present Letter	Previous reports	I_γ	$J_i^\pi \to J_f^\pi$	Coincidence(s)
^{76}Zn	602(9)	598.70(6) [43]	100(10)	$(2_1^+) \to 0^+_{\text{g.s.}}$	703, 1053 keV
	703(11)	697.69(7) [43]	72(7)	$(4_1^+) \to (2_1^+)$	602 keV
	1053(16)		33(4)		602 keV
^{78}Zn	740(11)	729.6(5) [42]	100(10)	$(2_1^+) \to 0^+_{\text{g.s.}}$	580, 902 keV
	902(14)	889.9(5) [42]	93(9)	$(4_1^+) \to (2_1^+)$	740 keV
	580(9)		14(2)		740 keV
	1271(19)		4(1)		
^{80}Zn	1497(22)[a]	1492(1) [30]	100(12)[b]	$(2_1^+) \to 0^+_{\text{g.s.}}$	482, 841, 1195 keV
	482(7)		60(6)	$(4_1^+) \to (2_1^+)$	841, 1195, 1497 keV
	841(13)		12(2)	$\text{X} \to (4_1^+)$	482, 1497 keV
	1195(18)		17(2)	$\text{X} \to (4_1^+)$	482, 1497 keV
	2627(39)[c]		3(1)	$\text{X} \to 0^+_{\text{g.s.}}$	
^{82}Zn	621(11)			$(2_1^+) \to 0^+_{\text{g.s.}}$	
^{82}Ge	1354(20)	1348.17(12) [45]	100(10)	$(2_1^+) \to 0^+_{\text{g.s.}}$	688, 934 keV
	934(14)	938.83(11) [45]	50(5)	$(4_1^+) \to (2_1^+)$	1354 keV
	688(11)		8(1)		1354 keV

[a] Value deduced from ^{9}Be(^{80}Zn,^{80}Zn+γ).
[b] Components of the 0.53- and 136-ps lifetimes are 33(4) and 67(7), respectively.
[c] Value deduced from $M_\gamma = 1$ events.

In addition, the $R_{4/2}$ ratio drops significantly at $N = 50$. These trends, therefore, suggest that $N = 50$ remains a good magic number in neutron-rich Zn isotopes. The shell-model calculations, discussed above, reproduce the systematic trends of the experimental results, and it is apparent that the MCSM calculations provide a better description. The relatively large discrepancy for $E(2_1^+)$ between the JUN45 interaction and experimental data at $N = 50$ may be attributed to the limited model space adopted for neutrons. Although the $E(2_1^+)$ values along the $N = 50$ isotonic chain [Fig. 5(b)] do not differ significantly from one another, $E(4_1^+)$ and $R_{4/2}$ for ^{80}Zn are notably lower than they are for other isotones. This may be interpreted as a development of multinucleon structures that reflect a decrease in collectivity as the number of valence nucleons is reduced approaching ^{78}Ni. Thus, the results of the present Letter highlight the robustness of the $N = 50$ magic number in exotic systems around doubly magic ^{78}Ni.

As discussed above, the spins of the low-lying excited states in ^{80}Zn can be interpreted in terms of the two-particle configurations. The fact that the first 4^+ state lies close in energy to the 2_1^+ level suggests that $(\pi f_{5/2})^2$ configurations are important because $(\pi p_{3/2})^2$ configurations can only generate states with spins as high as $2\hbar$. Indeed, according to the shell-model calculations, the main components of the wave functions of the $0^+_{\text{g.s.}}$, 2_1^+, and 4_1^+ states involve $(\pi f_{5/2})^2$ configurations. This suggests an inversion of the $\pi p_{3/2}$ and $\pi f_{5/2}$ proton single-particle orbitals in neutron-rich Zn isotopes, which is similar to the case of ^{75}Cu [29].

In summary, excited states in even-even nuclei in the vicinity of ^{78}Ni have been investigated via in-beam γ-ray spectroscopy with nucleon knockout reactions. New excited states in ^{80,82}Zn have been identified. The trends of $E(2_1^+)$ and $R_{4/2}$ indicate a persistent $N = 50$ magic number in neutron-rich Zn isotopes. The significant drop in $R_{4/2}$ at $N = 50$ suggests that the shell structure of ^{80}Zn is consistent with description of two-proton configurations with a ^{78}Ni core. Moreover, the low-lying 4_1^+ state in ^{80}Zn may indicate an inversion of the $\pi p_{3/2}$ and $\pi f_{5/2}$ single-particle energies. The results can be interpreted consistently in terms of robust magicity at $N = 50$ in exotic Zn isotopes, and may reflect the doubly magic shell structure of ^{78}Ni.

The authors thank the RIKEN Nishina Center accelerator staff and BigRIPS team for providing the intense, stable uranium beam, and for optimizing the radioactive beam. This work was supported by the RIKEN Junior Research Associate Program. D.S. acknowledges financial support from the Japan Society for the Promotion of Science under Grant No. 26 04327. The MCSM calculations were performed on the K computer at the RIKEN AICS (Project ID: hp140210 and hp150224). The present work was partly supported by the OTKA Contract No. K100835.

* yoshiaki.shiga@rikkyo.ac.jp
† Present address: Department of Physics, University of Hong Kong, Pokfulam Road, Hong Kong.
‡ Present address: Center for Nuclear Study, University of Tokyo, RIKEN campus, Wako, Saitama 351-0198, Japan.
§ Present address: Department of Physics, Tokyo Institute of Technology, Meguro, Tokyo 152-8551, Japan.
¶ Present address: Department of Science and Engineering, University of Tennessee, Knoxville, Tennessee 37996-1200, USA.
** Present address: Department of Physics, Tokyo University of Science, Noda, Chiba 278-8510, Japan.
†† Present address: KU Leuven, Instituut voor Kern-en Stralingsfysica, B-3001 Leuven, Belgium

[1] O. Haxel, J. H. D. Jensen, and H. E. Suess, Phys. Rev. **75**, 1766 (1949).
[2] M. Goeppert Mayer, Phys. Rev. **75**, 1969 (1949).
[3] A. Navin *et al.*, Phys. Rev. Lett. **85**, 266 (2000).
[4] H. Iwasaki *et al.*, Phys. Lett. B **481**, 7 (2000).
[5] H. Iwasaki *et al.*, Phys. Lett. B **491**, 8 (2000).
[6] T. Motobayashi *et al.*, Phys. Lett. B **346**, 9 (1995).
[7] C. M. Campbell *et al.*, Phys. Rev. Lett. **97**, 112501 (2006).
[8] B. Bastin *et al.*, Phys. Rev. Lett. **99**, 022503 (2007).
[9] S. Takeuchi *et al.*, Phys. Rev. Lett. **109**, 182501 (2012).
[10] R. Kanungo *et al.*, Phys. Rev. Lett. **102**, 152501 (2009).
[11] C. R. Hoffman *et al.*, Phys. Lett. B **672**, 17 (2009).
[12] A. Huck, G. Klotz, A. Knipper, C. Miehé, C. Richard-Serre, G. Walter, A. Poves, H. L. Ravn, and G. Marguier, Phys. Rev. C **31**, 2226 (1985).
[13] A. Gade *et al.*, Phys. Rev. C **74**, 021302(R) (2006).
[14] F. Wienholtz *et al.*, Nature (London) **498**, 346 (2013).
[15] R. V. F. Janssens *et al.*, Phys. Lett. B **546**, 55 (2002).
[16] D.-C. Dinca *et al.*, Phys. Rev. C **71**, 041302(R) (2005).
[17] J. I. Prisciandaro *et al.*, Phys. Lett. B **510**, 17 (2001).
[18] A. Bürger *et al.*, Phys. Lett. B **622**, 29 (2005).
[19] D. Steppenbeck *et al.*, Phys. Rev. Lett. **114**, 252501 (2015).
[20] M. Rosenbusch *et al.*, Phys. Rev. Lett. **114**, 202501 (2015).
[21] D. Steppenbeck *et al.*, Nature (London) **502**, 207 (2013).
[22] M. Arnould, S. Goriely, and K. Takahashi, Phys. Rep. **450**, 97 (2007).
[23] B. Pfeiffer, K.-L. Kratz, F.-K. Thielemann, and W. B. Walters, Nucl. Phys. A **693**, 282 (2001).
[24] J. Hakala *et al.*, Phys. Rev. Lett. **101**, 052502 (2008).
[25] Z. Y. Xu *et al.*, Phys. Rev. Lett. **113**, 032505 (2014).
[26] Y. Tsunoda, T. Otsuka, N. Shimizu, M. Honma, and Y. Utsuno, Phys. Rev. C **89**, 031301(R) (2014).
[27] K. Sieja and F. Nowacki, Phys. Rev. C **81**, 061303(R) (2010).
[28] T. Otsuka, T. Suzuki, R. Fujimoto, H. Grawe, and Y. Akaishi, Phys. Rev. Lett. **95**, 232502 (2005).
[29] K. T. Flanagan *et al.*, Phys. Rev. Lett. **103**, 142501 (2009).
[30] J. Van de Walle *et al.*, Phys. Rev. Lett. **99**, 142501 (2007).
[31] J. Van de Walle *et al.*, Phys. Rev. C **79**, 014309 (2009).
[32] M. Honma, T. Otsuka, T. Mizusaki, and M. Hjorth-Jensen, Phys. Rev. C **80**, 064323 (2009).
[33] T. Kubo *et al.*, Prog. Theor. Exp. Phys. **2012**, 03C003 (2012).
[34] S. Takeuchi, T. Motobayashi, Y. Togano, M. Matsushita, N. Aoi, K. Demichi, H. Hasegawa, and H. Murakami, Nucl. Instrum. Methods Phys. Res., Sect. A **763**, 596 (2014).
[35] S. Agostinelli *et al.*, Nucl. Instrum. Methods Phys. Res., Sect. A **506**, 250 (2003).
[36] http://www.nndc.bnl.gov/ .
[37] K. Yoneda *et al.*, Phys. Lett. B **499**, 233 (2001).
[38] P. Fallon *et al.*, Phys. Rev. C **81**, 041302 (2010).
[39] A. Gade *et al.*, Phys. Rev. C **81**, 064326 (2010).
[40] P. Doornenbal *et al.*, Phys. Rev. Lett. **111**, 212502 (2013).
[41] P. Doornenbal *et al.*, Nucl. Instrum. Methods Phys. Res., Sect. A **613**, 218 (2010).
[42] J. M. Daugas *et al.*, Phys. Lett. B **476**, 213 (2000).
[43] J. Van Roosbroeck *et al.*, Phys. Rev. C **71**, 054307 (2005).
[44] T. Rząca-Urban, W. Urban, J. L. Durell, A. G. Smith, and I. Ahmad, Phys. Rev. C **76**, 027302 (2007).
[45] J. A. Winger *et al.*, Phys. Rev. C **81**, 044303 (2010).
[46] J. J. Ressler *et al.*, Phys. Rev. C **69**, 034317 (2004).
[47] R. B. Cakirli, R. F. Casten, J. Jolie, and N. Warr, Phys. Rev. C **70**, 047302 (2004).